THE JOURNAL OF PHYSICAL CHEMISTRY B

Article

pubs.acs.org/JPCB

Excitonic Coupling in Linear and Trefoil Trimer Perylenediimide Molecules Probed by Single-Molecule Spectroscopy

Hyejin Yoo,[†] Shu Furumaki,[‡] Jaesung Yang,[†] Ji-Eun Lee,[†] Heejae Chung,[†] Tatsuya Oba,[‡] Hiroyuki Kobayashi,[‡] Boris Rybtchinski,[§] Thea M. Wilson,[§] Michael R. Wasielewski,*[,§] Martin Vacha,*[,‡] and Dongho Kim*[,†]

[†]Department of Chemistry, Yonsei University, Seoul 120-749, Korea

[‡]Department of Organic and Polymeric Materials, Tokyo Institute of Technology, Ookayama 2-12-1-S8, Meguro-ku, Tokyo 152-8552, Japan

[§]Department of Chemistry and Argonne-Northwestern Solar Energy Research (ANSER) Center, Northwestern University, Evanston, Illinois 60208-3113, United States

Supporting Information

ABSTRACT: Perylenediimide (PDI) molecules are promising building blocks for photophysical studies of electronic interactions within multichromophore arrays. Such PDI arrays are important materials for fabrication of molecular nanodevices such as organic light-emitting diodes, organic semiconductors, and biosensors because of their high photostability, chemical and physical inertness, electron affinity, and high tinctorial strength over the entire visible spectrum. In this work, PDIs have been organized into linear (**L3**) and trefoil (**T3**) trimer molecules and investigated by single-molecule fluorescence microscopy to probe the relationship between molecular structures and interchromophoric electronic interactions. We found a broad distribution of coupling strengths in both **L3** and **T3** and hence strong/weak coupling between PDI units by monitoring spectral peak shifts in single-molecule fluorescence spectra upon sequential photobleaching of each constituent chromophore. In addition, we used a wide-field defocused imaging technique to resolve heterogeneities in molecular structures of **L3** and **T3** embedded in a PMMA polymer matrix. A systematic comparison between the two sets of experimental results allowed us to infer the correlation between intermolecular interactions and molecular structures. Our results show control of the PDI intermolecular interactions using suitable multichromophoric structures.

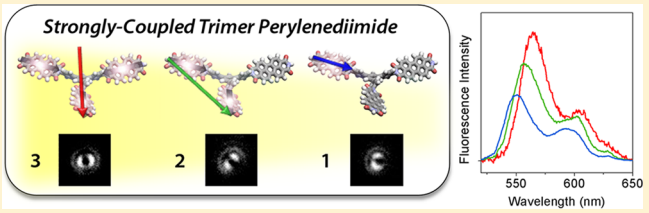

INTRODUCTION

Intermolecular interactions among constituent chromophores in multichromophoric molecular assemblies play a key role in determining their photophysical properties. Effective control of photophysical properties is a prerequisite for fabricating molecular photonic/electronic devices such as artificial light-harvesting systems,[1−3] photovoltaic devices,[4−7] organic light-emitting diodes,[8] and solar cells.[9] In molecular assemblies, generation of new electronic states by a close proximity of individual molecules causes the appearance of optical and electronic properties that are not observed in isolated chromophores, leading to their potential applications in functional organic electronics/photonics.[10] Much attention has been paid to the fundamental optical properties of various molecular complexes with the aim of revealing the nature of molecular interactions in relation to molecular structure, in particular, to the distances and angles between adjacent chromophores, and the influence of molecular structure on electronic communication in multichromophoric molecular assemblies.[11] Among them, covalently linked molecular arrays are one of the most suitable models to investigate interchromophoric interactions.

Perylenediimide (PDI) has been recognized as a nearly ideal chromophore for constructing multichromophoric architectures since it possesses high photochemical stability, electron affinity, and high fluorescence quantum yield.[12] We prepared two different PDI trimer molecules: one is a directly linked linear trimer (**L3**), and the other is a trefoil trimer (**T3**) with 1,3,5-triphenylbenzene linker (Chart 1). We explore the effect of molecular structure on interchromophoric interactions and the resultant photophysical properties by studying the molecular coupling strengths in **L3** and **T3** and comparing the coupling strengths with heterogeneity of each molecular structure determined by its nanoenvironment.

Previous ensemble spectroscopic studies on the directly linked linear trimer[13] reported that the collective excited state of the system mediated by exciton coupling can enhance fluorescence emission. Furthermore, Wasielewski et al. found that PDI chromophores of the trefoil[14] as well as the linear trimer are electronically coupled to show bathochromic shifts in

Received: July 26, 2012
Revised: September 23, 2012
Published: September 24, 2012

Chart 1. Molecular Structures of Linear (L3) and Trefoil (T3) Trimers

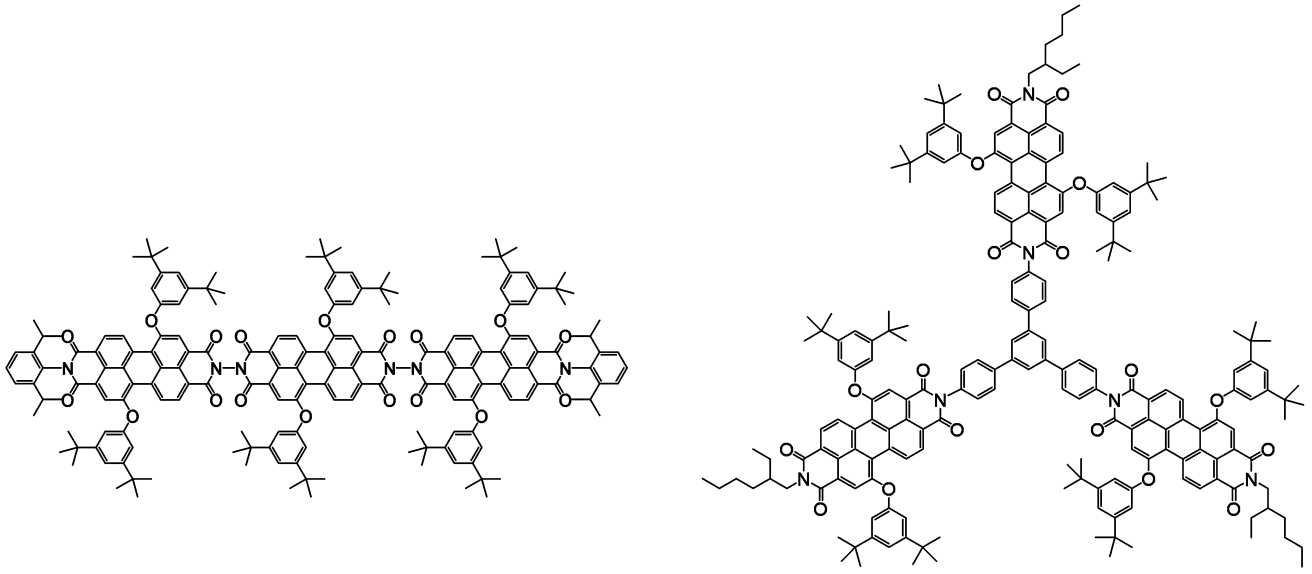

the absorption and emission spectra as compared with those of the monomer. Although ensemble measurements are essential in the investigation of molecular properties, they often preclude detailed information on a single-molecule level by averaging over all measured observables. As a consequence, the ensemble properties of multichromophores conceal a unique contribution by each constituent chromophore to the intermolecular coupling as well as the distribution of individual multichromophoric properties.

Single-molecule detection techniques have proven useful to obtain detailed molecular information such as the distribution of single-molecule parameters. In the case of multichromophores, intensity time traces and changes in the photophysical parameters upon photobleaching provide invaluable information on the individual constituent chromophores and their interactions. In this work, we employed single-molecule fluorescence microscopy (SMFS) to unveil the differences in molecular interactions between **L3** and **T3** in relation to their molecular structures. Single-molecule fluorescence spectra and wide-field defocused imaging manifest fluorescence spectral dynamics (such as spectral shifts), changes in emission intensity, and distribution of molecular orientations (heterogeneous molecular structures) of **L3** and **T3** single molecules. We demonstrated by single-molecule experiments and model calculations that the fluorescence spectral shift of the **L3** trimer is mainly determined by the intermolecular distance and the angle-dependent dipole−dipole interactions. On the other hand, the **T3** trimer shows spectral shifts that are not explainable by pure dipole−dipole interactions of the constituent chromophores and indicate that an electronic contribution from the triphenylbenzene linker plays a role in the interchromophoric coupling. The coupling strengths were compared with individual heterogeneous molecular structures obtained from wide-field defocused imaging, and the comparison showed a good correlation between the coupling and the expected structural features.

EXPERIMENTAL SECTION

Sample Preparation for the Single-Molecule Fluorescence Imaging of L3 and T3. Diluted toluene solutions of **L3** and **T3** are mixed with a toluene solution of the matrix polymer which is a 2 wt % toluene solution of poly(methyl methacrylate) (PMMA). The final concentration of **L3** and **T3** in the solution was 1×10^{-10} M. The solution was spin coated onto thoroughly cleaned microscope coverslips. The thickness of the film is on the order of ∼100 nm.

Single-Molecule Spectroscopy. Single-molecule experiments were performed using a wide-field fluorescence microscope consisting of an inverted optical microscope (IX71, Olympus) equipped with an oil immersion objective (1.3 NA, ×100, Plan Fluorite Olympus) and an EM CCD camera (Andor, iXon). For excitation, the 488 nm light from the Ar−Kr ion laser (Innova 70C, Coherent) was used. The collimated, circular polarized laser beam was sent to the input port of the epi-fluorescence microscope after passing a beam expander. Fluorescence spectra of single molecules were measured with a CCD coupled imaging spectrograph (Bunko Keiki CLP-50). Recorded spectra were corrected for background. Determination of the peak position of each spectrum was done by fitting with Gaussian functions. To obtain the defocused images, the sample plane was shifted by 0.9 μm toward the objective from the focus position and the image was further magnified 3.6 times with a relay lens before the CCD camera. Integration time per frame was 1 s. Defocused images thus obtained were analyzed using a routine written in MatLab software, in order to determine molecular orientation in each image frame. Images were first analyzed using a pattern-matching routine to determine roughly the molecular orientation in each image frame by calculating two-dimensional correlation coefficients (r) of the defocused images obtained experimentally (A) and theoretically (B) using the equation

$$r = \frac{\sum_m \sum_n (A_{mn} - \bar{A})(B_{mn} - \bar{B})}{\sqrt{(\sum_m \sum_n (A_{mn} - \bar{A})^2)(\sum_m \sum_n (B_{mn} - \bar{B})^2)}}$$

where $\bar{A}$ and $\bar{B}$ are the means of A and B, respectively. All measurements were done at room temperature under ambient atmosphere.

Ensemble Spectroscopy. Steady-state absorption spectra were taken in a UV−vis−near-IR spectrometer (Cary model 5000, Varian), and steady-state fluorescence spectra were obtained in a fluorescence spectrometer (model F-2500,

dx.doi.org/10.1021/jp307394x | J. Phys. Chem. B 2012, 116, 12878−12886

Hitachi) at an excitation wavelength of 490 nm. All spectra were measured in toluene (Aldrich, anhydrous, 99.9%, spectrophotometric grade).

RESULTS AND DISCUSSION

Structures and Ensemble Measurements. Molecular structures of **L3** and **T3** are given in Chart 1. While PDIs with two phenoxy substituents are directly linked in a linear fashion in **L3**, **T3** exhibits a trefoil structure due to the triphenylbenzene linker between the neighboring PDI chromophores. The normalized absorption and fluorescence spectra of the PDI monomer, **L3** and **T3**, are shown in Figure 1. The red-shifted absorption and fluorescence spectra of PDI trimers (**L3** and **T3**) compared to those of the monomer indicate that there is electronic communication between the PDI units in the trimers. In the directly linked linear trimer (**L3**), the exciton is likely to be delocalized over the three PDI units because of strong interactions through J-type exciton coupling. On the other hand, the three PDI units in trefoil trimer (**T3**) are well separated and supposedly weakly coupled because their transition dipole moments are not oriented in parallel and the interchromophoric distance is relatively large. As a consequence, absorption and fluorescence spectra of **L3** show a larger red shift than those of **T3**. Absorption and emission maxima are in Table 1. Moreover, in fluorescence lifetime measurements, **T3** shows a fluorescence lifetime (4.2 ns) similar to that of PDI monomer (4.6 ns) while the lifetime of **L3** is shorter (3.1 ns) (Figure S1, Supporting Information). This indicates that the three PDI chromophores are more strongly coupled in **L3**, a result which is consistent with the bathochromic shift in the absorption and emission spectra of **L3** as mentioned above.

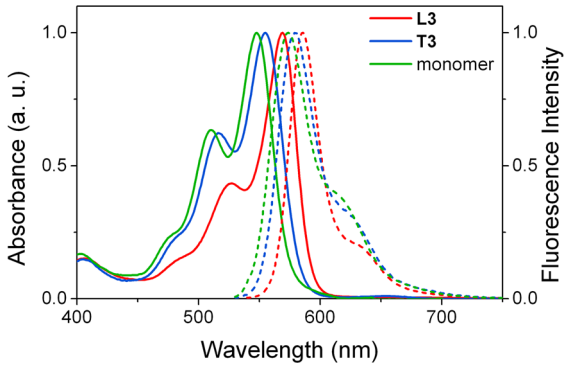

Figure 1. Steady-state absorption (solid) and fluorescence (dashed) spectra of PDI monomer (green), **L3** (red), and **T3** (blue). J-type exciton coupling of **L3** carries more intense transition to the lower energy exciton state. Both spectra of **T3** are slightly red shifted as compared with those of PDI monomer. All spectra were measured in toluene.

Under such situation, two limiting cases can be distinguished for the molecular interactions in PDI multichromophoric system. First, when PDI molecules have initially the same transition frequencies and orientations and are close to each other, the strong excitonic coupling between PDI units results in a Davydov shift/splitting[15] of the absorption spectrum and an enhanced emission (superradiance)[16] with a shorter fluorescence lifetime than the original excited state lifetime of PDI monomer. Herein, the super-radiant PDI multichromophore has a large dipole moment induced by the sum of the transition dipole moments of three PDI units (J-type exciton trimer). Second, if the coherence of the molecular system is lowered by phononic interactions with the matrix or longer distance between molecules, molecular interactions turn into weak coupling which does not alter the absorption spectrum but, however, allows a simple energy transfer. This energy transfer process has been described as Föster resonance energy transfer which arises from dipole−dipole interactions between the electronic states of the donor and acceptor.[17] In this situation, constituting PDI units of multichromophore emit monomer-type fluorescence from the localized state. Both strong and weak coupling interactions of artificial as well as natural multichromophoric systems have been studied extensively in recent years.[11d,18] In this work, we focused our attention on the degree of coherency and coupling strength of PDI trimer depending on the molecular geometry embedded in the nanoenvironment.

Fluorescence Spectra of L3 and T3 at the Single-Molecule Level. Because both **L3** and **T3** show red-shifted fluorescence spectra in the bulk, we can expect differences in the maximum peak positions of single-molecule spectra corresponding to the trimer, dimer, and monomer state of **L3** and **T3**, and these spectra should be revealed in that order during sequential photobleaching. We measured the fluorescence spectra of single molecules and analyzed spectral shifts during subsequent photobleaching of the three PDI units of trimers to probe the decrease in exciton delocalization between the PDI units in **L3** and **T3**. As a reference, we measured the

Table 1. Absorption and Emission Maxima (λ_{abs} and λ_{em}), Average Peak Positions of Trimer, Dimer, and Monomer Single-Molecule Spectra, and Experimental and Theoretical Spectral Shifts from Trimer and Dimer to Monomer State of L3 and T3

	absorption and emission maxima (nm)[a]		average peak position (cm^{-1})[b]			spectral shift (cm^{-1})			
						trimer−monomer		dimer−monomer	
	λ_{abs}	λ_{em}	trimer	dimer	monomer	exp.[c]	theo.[d]	exp.	theo.
L3	569	586	17 545	17 782	18 271	726	596	489	403
T3	555	579	17 684	17 937	18 146	462	115	240	67
PDI	548	574			18 198				

[a]Measured in Figure 1. [b]Calculated by summing the maximum peak position values in the fluorescence spectra of the same molecular state of **L3** and **T3**. In a large number of lifetime data sets, each average spectral peak might converge in the confidence interval (±94−164) within 95% confidence level (Table S2 in the Supporting Information). Although the number of sample molecules is relatively small, the error range does not influence the overall tendency of the results, i.e., the blue-shifted spectral peak in the order of trimer, dimer, and monomer. [c]Experimental spectral shifts were obtained by subtracting the maximum spectral peak position of trimer or dimer from that of monomer state. [d]Theoretical spectral peak shifts were estimated by calculating the coupling strength among the constituent chromophores. For detailed information, refer the Supporting Information.

dx.doi.org/10.1021/jp307394x | J. Phys. Chem. B 2012, 116, 12878−12886

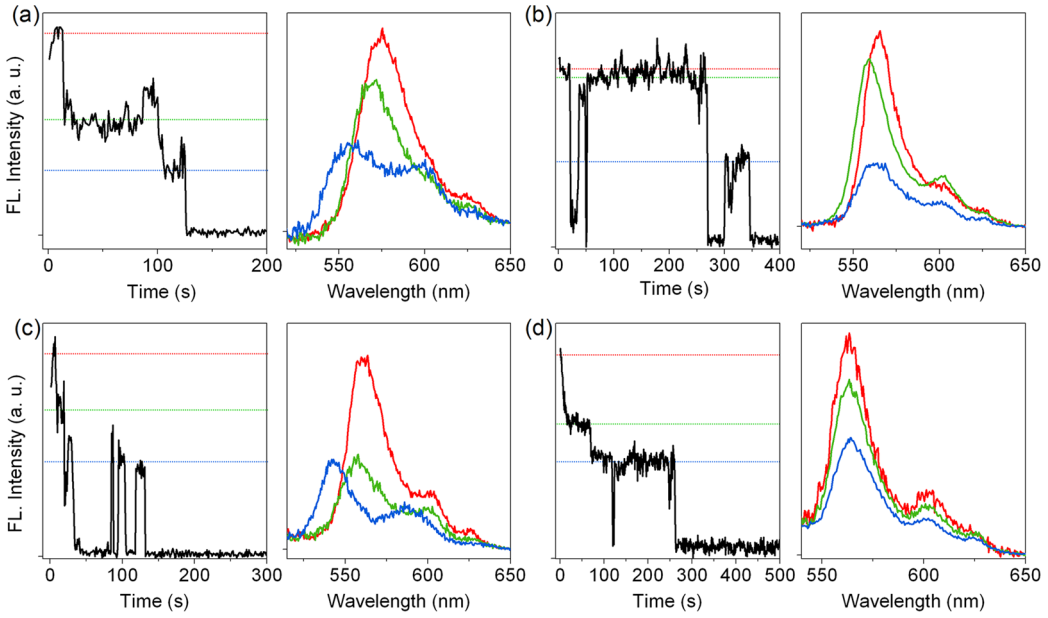

Figure 2. Representative fluorescence intensity trajectories (FITs) and corresponding fluorescence spectra of **L3**. Each spectrum is averaged from a bunch of single-molecule spectra in the same intensity level which were measured for 1 s. FITs are extracted by integration of every spectrum as a function of wavenumber. Spectra observed at the first, second, and third intensity levels are displayed as red, green, and blue lines, respectively. Spectral shift behaviors are categorized into four types: continuing shifts (a), single shift (b, c), and no shift (d).

fluorescence spectra of single PDI monomers. All PDI monomer molecules show the same spectral shapes in the entire fluorescence intensity trajectories (FITs, Figure S2, Supporting Information). In contrast, for **L3** and **T3** the spectral features change remarkably depending on the steps of FITs, as seen in Figures 2 and 3. All series of fluorescence spectra were measured with a bin time of 1 s, and the FITs were obtained by integrating the intensity of each fluorescence spectrum. Representative spectral curves (such as those in Figure 2) are obtained as average spectra at each intensity level in the FIT. Spectra observed at the trimer, dimer, and monomer intensity levels are displayed as red, green, and blue lines, respectively. For a systematic analysis, we selected trimer molecules showing three distinct intensity levels in the FITs.

In the case of **L3**, among the 37 molecules measured 16 molecules show sequentially blue-shifted fluorescence spectra (Figure 2a) during photobleaching, indicating that the PDI units are strongly coupled.[19−22] These molecules likely follow the photobleaching sequence as described in Figure S3a, Supporting Information, i.e., starting from the terminal PDI unit. In this case, the intermediate dimer also emits red-shifted fluorescence as compared with monomer as a result of exciton delocalization. Representative trimer and dimer emission spectra in Figure 2a are relatively broad with a smaller contribution of the second vibronic band, while the monomer spectrum has two clear vibronic bands. Second, the fluorescence spectra of 6 molecules of **L3** exhibit a blue shift during the first photobleaching event and remain unchanged in spectral position during the second photobleaching step as seen in Figure 2b. Because the peak position of the fluorescence spectrum of the dimer state is similar to that of the monomer one, we conclude that the two remaining emitting PDI units are not coupled. In this case, excitonic coupling among the three PDI units may be broken during the initial photobleaching event which occurs on the central PDI unit, and the uncoupled chromophores at opposite ends emit monomer fluorescence separately, resulting only in a 2-fold increase in fluorescence intensity as compared with monomer. Twelve molecules of **L3** show a trend in the spectral shift opposite to the aforementioned molecules, that is, the fluorescence spectra mainly change during the second photobleaching event, as shown in Figure 2c. In this case, initially only two adjacent (rather than three) PDI units of **L3** are strongly coupled (see Figure S3c, Supporting Information). Therefore, the fluorescence intensity decreases during the first step, without change in peak position when the molecular state changes from trimer to dimer.

Most of the **L3** molecules exhibit spectral shifts because two or three chromophores of **L3** interact strongly. However, no spectral changes between photobleaching events have also been observed for 3 molecules of **L3** (Figure 2d), because the three PDI chromophores in these **L3** molecules are interacting weakly and are excited and emit fluorescence separately like isolated monomers.

We next carried out the same experiment for **T3**. Figure 3 shows the single-molecule fluorescence spectra of **T3** at each intensity level of FITs. All 41 measured FITs are categorized according to the type of spectral shift, in the same manner as **L3**. Nine molecules of **T3** show sequential spectral shifts to shorter wavelength in the order of trimer, dimer, and monomer, as seen in Figure 3a. The nonparallel orientation of constituent PDI units in **T3** with an interchromophoric angle of ∼120° as well as the long interchromophoric distance due to the presence of the triphenylbenzene linker are expected to diminish the coupling strength in **T3**. Despite these facts, the PDI chromophores of **T3** are efficiently coupled with each other and the fluorescence spectra of trimer and dimer are red shifted compared with that of monomer. These molecules likely have near-perfect trefoil structure which is causing equal interactions between the three PDI chromophores. The conceptual illustration with respect to the photobleaching process is displayed in Figure S3e, Supporting Information.

dx.doi.org/10.1021/jp307394x | J. Phys. Chem. B 2012, 116, 12878−12886

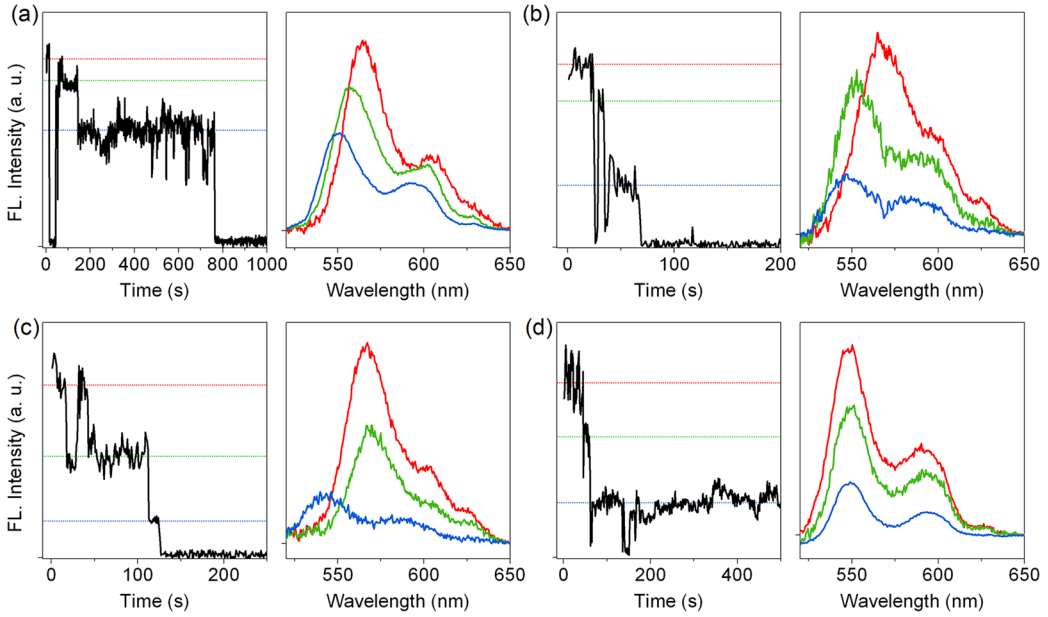

Figure 3. Representative fluorescence intensity trajectories (FITs) and corresponding spectra of **T3**. Like **L3**, **T3** molecules also show four types of spectral shift trends according to the structure and interaction among constituent PDI units.

More than one-half of **T3** molecules exhibit a spectral blue shift only once during sequential photobleaching. These **T3** molecules may have distorted structures with intermolecular angles larger or smaller than 120°, due to the influence of different nanoenvironments. If two PDI molecules come closer due to the small angle between them, only these two PDIs will strongly interact in **T3**. In this case, we can find two trends in the spectral shifts during the photobleaching processes. First, for 15 molecules the maximum peak positions of fluorescence spectra move to higher energy during the first photobleaching step, as seen in Figure 3b. When one of two strongly interacting PDIs is photobleached, the coherent coupling between the two chromophores is broken, and as a consequence, the fluorescence spectrum of the dimer is shifted to shorter wavelength (see Figure S3f, Supporting Information). Because the remaining two PDI molecules interact weakly, there is no spectral change in going from dimer to monomer state. On the other hand, seven molecules of **T3** show spectral peak shifts only during the second photobleaching step (Figure 3c). During the initial step, photobleaching of a noninteracting PDI monomer which does not participate in emission but only in the absorption process (see Figure S3g, Supporting Information) has no effect on the spectral peak position of the remaining strongly interacting dimer. In the second step, the fluorescence spectrum is shifted to shorter wavelength due to disruption of the coherent coupling.

Similar to the case of **L3** molecules, 10 molecules of **T3** also show little difference in the fluorescence spectral peak position during photobleaching (Figure 3d). PDI chromophores in these **T3** molecules are weakly coupled and emit fluorescence independently. Thus, the fluorescence spectrum of weakly coupled **T3** is positioned at higher energy compared with that of strongly coupled **T3**. The corresponding photobleaching mechanism is illustrated in Figure S3h, Supporting Information.

While the majority of **L3** molecules show sequential fluorescence spectral shift behavior, the fractions of **T3** molecules that exhibit shifted and nonshifted fluorescence spectra are similar. This fact supports the assertion that PDI chromophores in **L3** are more strongly coupled than in **T3** due to the well-defined linear structure of **L3** which provides better conditions to enhance the coherent coupling among the PDI transition dipole moments. In addition, both **L3** and **T3** show various trends in spectral shift because the intermolecular coupling strength and resulting spectral shift depend on the nanoenvironments surrounding the molecules.

Absorption spectra of J-aggregate molecular species generally show not only spectral red shifts but also enhanced 0−0 emission as compared with that of the constituent monomer.[15b,23] Figure 4 shows the effect of exciton delocalization on the relative strength of the 0−0 vibronic transition. Fluorescence spectra of strongly coupled **L3** are sequentially blue shifted, and the intensity of the 0−0 emission band decreases simultaneously in the FITs. As a result, the vibronic structure which is smoothed in the first fluorescence spectrum becomes distinct in the third spectrum. Quantitatively, the 0−0 to 1−0 vibronic band intensity ratio (I_{0-0}/I_{1-0}) decreases from 3.3 to 2.2 and 1.2 (Figure 4a). In contrast, weakly coupled **L3** shows unchanged spectral peak position and intensity ratio. In Figure 4b, the vibronic components are clearly distinguished with nearly the same I_{0-0}/I_{1-0} values of 3.9, 4.0, and 3.9 in the three steps in FITs, respectively. Therefore, these spectral features corroborate the aforementioned results about the relationship between coupling strength and spectral shift. Although **T3** does not exhibit a perfect J-type structure, it follows a decreasing tendency in the I_{0-0}/I_{1-0} intensity ratio upon sequential photobleaching of the strongly coupled trimer. In Figure 3a, for example, the I_{0-0}/I_{1-0} value decreases from 2.7 to 2.3 and to 2.1 in the three spectra corresponding to the three intensity levels of FITs. The intensity ratio histogram exhibits the tendency of decreasing I_{0-0}/I_{1-0} values in J-type aggregated **L3** in comparison with **T3** (see Figure S4, Supporting Information).

For further analysis, we collected all peak position data measured from the three spectra of each single molecule and summarized them into frequency histograms in Figure 5 (see also Figure S5, Supporting Information). While the three

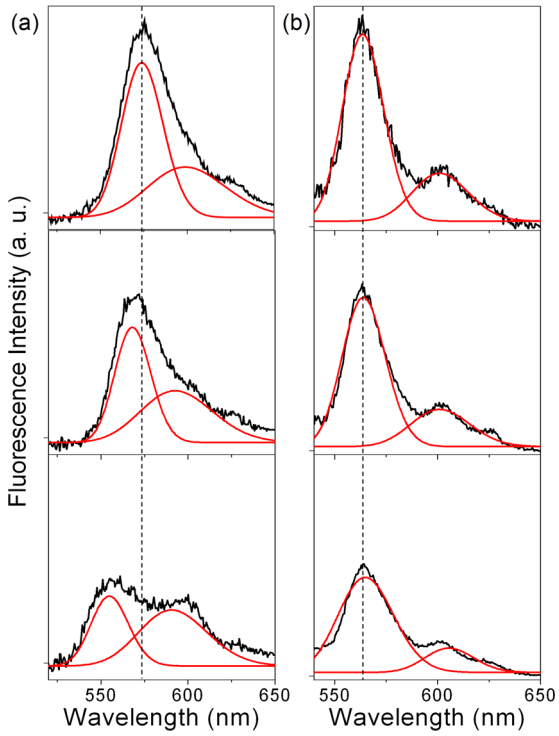

Figure 4. Fluorescence spectra of **L3** fitted with two Gaussian distributions. From top to bottom, each spectrum corresponds to trimer, dimer, and monomer emission, respectively. a and b, which are derived from Figure 2a and 2d, represent the relationship between coupling strength and vibronic band intensity ratio. I_{0-0}/I_{1-0} are 3.3, 2.2, 1.2 (a) and 3.9, 4.0, 3.9 (b), respectively. Dashed line indicates the maximum peak position of the trimer emission spectrum.

distributions of **L3** are clearly separated, those of **T3** are significantly overlapping. Moreover, the intervals between three distributions of **T3** are smaller than those of **L3**, which is in good agreement with larger spectral shifts in **L3**. Overall, **L3** shows an obvious trend of spectral peak shift as compared with **T3**, which is consistent with the ensemble fluorescence spectra.

The mean values of spectral peak positions and spectral shifts in going from trimer to dimer and monomer states in FITs are listed in Table 1. The transition energies of linear trimer and dimer states of **L3** are lower than those of trefoil trimer and dimer states of **T3**. By subtracting the trimer and dimer mean peak position values from those of the monomer, we estimated mean experimental spectral displacements between trimer, dimer, and monomer emission maxima of **L3** and **T3**. Overall, the shift values in the spectra of **L3** are larger than those of **T3**, which is in a good agreement with the above results. In addition, theoretical values[24] were also obtained by calculating the transition dipole coupling energy between the two transition dipoles for the linear and trefoil geometries. We employed the matrix diagonalization method[25] to calculate the coupling strength of the trimers using matrix elements consisting of the coupling energies between the transition dipoles. While the experimental and theoretical spectral shift values for **L3** show a reasonable agreement, the experimental peak shift values of **T3** are significantly larger than the theoretical ones. The reason for this discrepancy most likely results from the polarizability of the phenyl linker in **T3**, which enhances the dipole−dipole coupling and mitigates steric hindrances between PDI moieties due to the large interchromophoric distance.[26,27]

Defocused Images of L3 and T3 Single Molecules. To obtain information about the orientation of transition dipole moments of individual chromophores in **L3** and **T3**, we measured defocused images of **L3** and **T3** at the single-molecule level and analyzed in- and out-of-plane angle changes during the photobleaching process. Individual chromophores emit anisotropic fluorescence depending on the orientation of their transition dipole moments.[28−30] Thus, we can infer the molecular structures of **L3** and **T3** as well as the orientation of newly generated transition dipole moments of trimer and dimer states by analyzing changes of defocused images in relation to the sequential photobleaching processes. Prior to defocused imaging experiments, we also found that **L3** shows no variations in fluorescence polarization traces due to the parallel alignment of three chromophores along the long molecular axis of **L3**. On the other hand, the polarization of **T3** changes significantly as each chromophore is photobleached in the order as depicted in Figure S6, Supporting Information.

In the defocused imaging experiments, the FITs are plotted by subtracting the background signal from the integrated intensity of all of the defocused emission patterns with a bin time of 1 s. To evaluate a change in the orientation of transition dipole moments in the trimer molecules during photobleaching, we analyzed only those FITs which showed three distinct intensity levels.

Defocused images of **L3** show that the majority of molecules have similar patterns at all three intensity levels. The representative **L3** molecule in Figure 6 shows that there is no significant difference in the angles of 85° for out-of-plane and 125° for in-plane among the three images. Because **L3** molecule has a linear structure, the differences in angles between two PDI units are close to 0°.

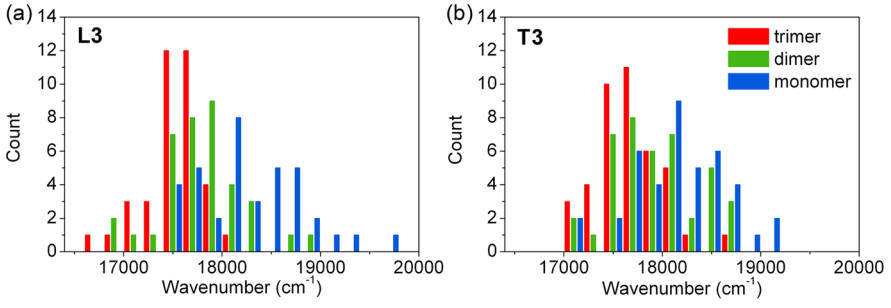

Figure 5. Histograms of spectral peak position at each level of FITs in **L3** (a) and **T3** (b). Individual points are extracted from three spectra of each single molecule. Subdistributions are indicated by red, green, and blue for trimer, dimer, and monomer, respectively.

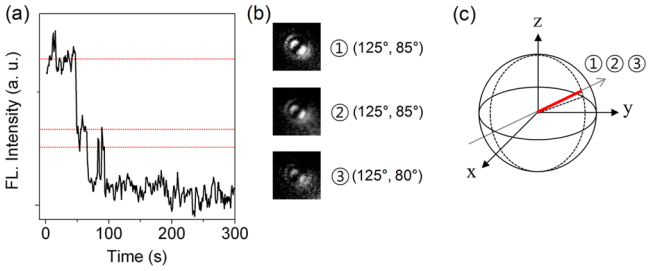

Figure 6. Representative fluorescence intensity trajectory (a) of **L3** and defocused images (b) measured at each intensity level. On the basis of calculated in-plane and out-of-plane angles, molecular orientation can be displayed as vector components on polar coordinate (c). In the case of **L3**, three chromophores are arranged in parallel.

Compared with **L3**, **T3** molecules show a variety of emission patterns. Two kinds of variations of defocused images are depicted in Figure 7. In Figure 7a and 7b, the strongly coupled **T3** molecule exhibits emission patterns corresponding to a linear dipole moment at each intensity level. We matched these patterns directly with the theoretically calculated defocused emission patterns. The defined angles of the transition dipole moments are 75°, 225°, and 185° for in plane and 80°, 70°, and 60° for out of plane, respectively. The arrows in Figure 7c indicate the orientations of the transition dipole moments of trimer, dimer, and monomer states, respectively. We can estimate the transition dipole moments of the strongly coupled trimer and dimer states in the ideal molecular structure of **T3** with interchromophoric angles of 120°, according to the contributions of each transition dipole moment of the constituent PDI monomers which was calculated by the matrix diagonalization method as aforementioned. If the PDI units of **T3** are photobleached in the particular order as seen in Figure S7, Supporting Information, the transition dipole moment can be expected to rotate by ~20° and ~40° during the first and second photobleaching events, respectively. In fact, the transition dipole moment in Figure 7c rotates by angles of 20° and 36°, respectively, during the two photobleaching events of PDI units. This experimental result coincides with the estimated values. Thus, in this case, the **T3** molecule which behaves as a single quantum system emits the fluorescence from the lowest energy exciton states generated by the strong coupling of three and two PDI units at the first and second intensity levels of FIT, respectively.

In Figure 7d and 7e, the emission pattern at the first intensity level exhibits a circular shape which corresponds to the linear combination of the emission from three PDI units in weakly coupled **T3** molecule. To determine the orientation of each PDI unit, the emission pattern in the second (third) step was subtracted from the one in the previous step. With the calculated orientations of transition dipole moments of subtracted patterns observed in three intensity levels in FITs, we can sketch the molecular structure. Three PDI units have the orientation angles of 275°, 145°, and 30° for in plane and 90°, 90°, and 80° for out of plane, respectively. In this case, the three interchromophoric angles between the PDI units (130°, 115°, 115°) are close to 120° (Figure 7f), in good agreement with an ideal molecular structure of **T3**. This example demonstrates that from analyzing sequential emission patterns we can infer the structures of molecules embedded in different environments. Besides, we can retrieve information on molecular excited states indirectly; for example, when the energy levels of excited states of three PDI units as described in Figure 7e are similar, successive energy hopping among three chromophores causes them to emit fluorescence alternatively.[31] Both strongly and weakly coupled **T3** molecules can be regarded as typical cases by static analysis. The molecular angle histogram of **T3** shows two kinds of distributions correspond-

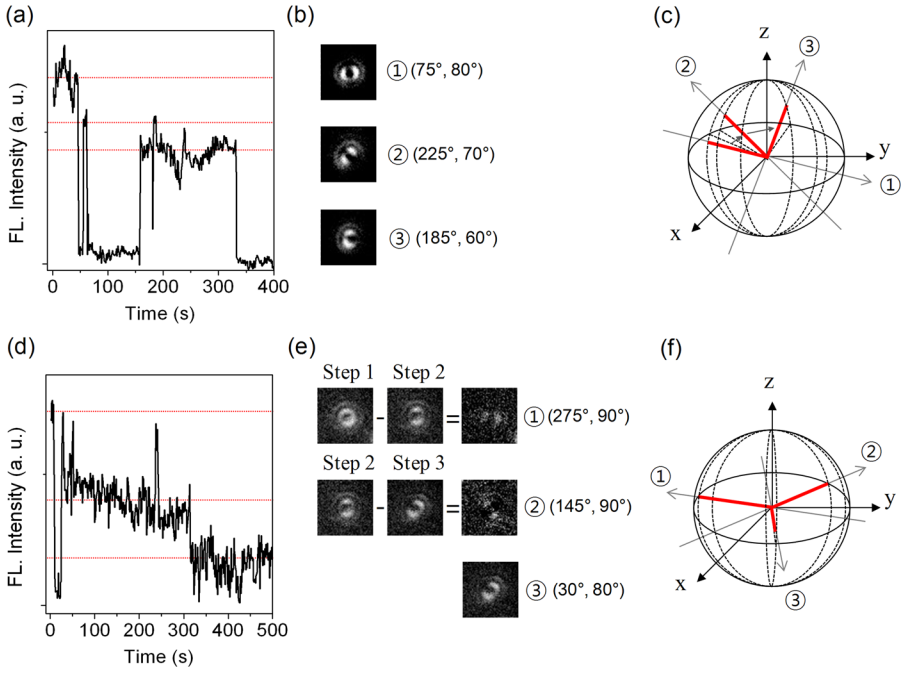

Figure 7. Fluorescence intensity trajectories (FITs) and corresponding defocused images of **T3**. FITs (a, d) are plotted by the integrated intensity of each defocused image measured in a bin time with 1 s (b, e). Calculated orientations of each PDI unit and expected molecular alignments are depicted as arrows and red bars, respectively, in polar coordinates (c, f). Molecular angles between two chromophores, 1–2, 2–3, and 3–1 = 130°, 115°, 115° (f).

dx.doi.org/10.1021/jp307394x | J. Phys. Chem. B 2012, 116, 12878–12886

ing to strong coupling with small angles and weak coupling with molecular angles of around 120°, respectively (Figure S9, Supporting Information).

Besides these results, more than one-half of **T3** molecules show one or two kinds of emission patterns in spite of three-step intensity traces as displayed in Figure S8, Supporting Information. In Figure S8a and S8b, Supporting Information, the structure of the **T3** molecule deviates from the ideal one with large discrepancies in interchromophoric angle (i.e., 100°). This torsional structure coincides with the result of the spectrum analysis (Figure 3b and 3c). Additionally, three linear emission patterns in Figure S8e, Supporting Information, are the same because energy transfer processes between PDI units allow preferential emission from the chromophore which is in the lowest energy state.

Now we consider the single-molecule fluorescence spectra in relation to the defocused imaging analysis. First, the strongly coupled trimers showing sequential spectral shifts to higher energy upon photobleaching of each PDI chromophore would correspond to ideal geometries, such as exactly linear and trefoil structures for **L3** and **T3** with interchromophoric angles of 0° and 120°, respectively. The three PDI chromophores in the well-defined structures interact strongly, thus exhibiting two-step sequential spectral shifts and rotations of the transition dipole moment by small angles of 20° and 40° in the overall fluorescence emission. In other words, we observed the strongly coupled **L3** and **T3** which generate new energy states and transition dipole moments in trimer and dimer levels from both single-molecule fluorescence spectra and wide-field defocused images. Second, the weakly coupled trimers (**T3**) have ideal molecular structures with interchromophoric angles of ∼120°. In addition, they show different fluorescence dynamics from the strongly coupled trimer, constant peak positions in fluorescence spectra and fluorescence from three isolated emitting monomers as observed by defocused images. On the other hand, partially coupled trimers, especially **T3**, are expected to have torsional and kinked structures. Here, we directly unveiled the existence of such torsional structures of **T3** with nonideal interchromophoric angles. When two chromophores in **T3** become closer in the torsional structure, they can be strongly coupled without influence from the remaining monomer, and as a consequence, such types of **T3** behave as a partially coupled system consisting of dimer and monomer. As a result, the fluorescence spectra shift to higher energy in a single step during the photobleaching sequence, as seen in Figure 3b and 3c. On the basis of a comparative analysis between the fluorescence spectrum and defocused imaging, we directly confirmed that the interchromophoric interactions depend on the molecular structures as well as the molecular nanoenvironment. Such strongly, weakly, and partially coupled trimer systems have been resolved by probing single-molecule fluorescence dynamics.

CONCLUSIONS

In this study, we elucidated molecular structure-dependent coherent coupling between the PDI units within **L3** and **T3** on the single-molecule level by analyzing the spectral peak shift, vibronic band intensity ratio, and change in the orientation of the transition dipole moments. Our single-molecule studies reveal the existence of not only strongly coupled PDI trimers but also weakly coupled ones, which are difficult to be observed by ensemble measurements. While the strongly coupled PDI trimers show blue-shifted spectra in going from trimer to monomer, the weakly coupled PDI trimers exhibit unchanged spectra except for a decrease in fluorescence intensity. **L3** follows more assiduously the spectral peak shift behavior because **L3** has a J-type conformation and a short distance between the constituent PDI units to enhance the molecular coupling. The coupling strength of **T3** is larger than expected due to the electronic contribution of the phenyl linker and the symmetric trefoil structure. Furthermore, in wide-field defocused imaging measurements, we confirmed the linear structure of **L3** and the trefoil structure of **T3** by monitoring the change of emission spatial patterns during stepwise photobleaching processes. Accordingly, the comparative studies on **L3** and **T3** in terms of both molecular structures and interactions provide important information on the coupling strengths of the constituent units in multichromophoric systems. The coupling strength is determined by the molecular structure (i.e., the distance and angle between molecular units) which in turn is influenced by the heterogeneous surrounding matrix. Thus, investigation of the relationship between the molecular structure and the photophysical properties of molecular arrays of different shapes can guide our designs of molecular assemblies for potential applications as effective photonic devices.

ASSOCIATED CONTENT

Supporting Information

Detailed description of the theoretical coupling strength, fluorescence decay profiles, hypothetical illustrations for photobleaching processes, polarization trajectories, expected transition dipole moments of strongly coupled **T3**, and additional defocused images of **T3**. This material is available free of charge via the Internet at http://pubs.acs.org.

AUTHOR INFORMATION

Corresponding Author

*E-mail: dongho@yonsei.ac.kr; vacha.m.aa@m.titech.ac.jp; m-wasielewski@northwestern.edu.

Notes

The authors declare no competing financial interest.

ACKNOWLEDGMENTS

The authors thank Dr. Satoshi Habuchi (currently at KAUST, Saudi Arabia) for helpful discussions. This research was financially supported by World Class University (R32-2010-000-10217) and Midcareer Researcher (2010-0029668) Programs from the Ministry of Education, Science, and Technology (MEST) of Korea (D.K.), by a Grant-in-Aid for Scientific Research No. 23651107 of the Japan Society for the Promotion of Science (M.V.), and by a Research Grant of Ogasawara Foundation (M.V.). Research at Northwestern University was supported by the Chemical Sciences, Geosciences, and Biosciences Division, Office of Basic Energy Sciences, DOE under grant no. DE-FG02-99ER14999 (M.R.W.).

REFERENCES

(1) Flors, C.; et al. *J. Phys. Chem. C* **2007**, *111*, 4861−4870.
(2) De Schryver, F. C.; Vosch, T.; Cotlet, M.; van der Auweraer, M.; Müllen, K.; Hofkens, J. *Acc. Chem. Res.* **2005**, *38*, 514−522.
(3) Yoo, H.; Yang, J.; Nakamura, Y.; Aratani, N.; Osuka, A.; Kim, D. *J. Am. Chem. Soc.* **2009**, *131*, 1488−1494.
(4) Wang, Y.; Chen, Y.; Li, R.; Wang, S.; Su, W.; Ma, P.; Wasielewski, M. R.; Li, X.; Jiang, J. *Langmuir* **2007**, *23*, 5836−5842.

(5) Dimitrakopoulos, C. D.; Malenfant, P. R. L. *Adv. Mater.* **2002**, *14*, 99−117.
(6) Chen, Z.; Stepanenko, V.; Dehm, V.; Prins, P.; Siebbeles, L. D. A.; Seibt, J.; Marquetand, P.; Engel, V.; Würthner, F. *Chem.—Eur. J.* **2007**, *13*, 436−449.
(7) Horowitz, G.; Kouki, F.; Spearman, P.; Fichou, D.; Nogues, C.; Pan, X.; Garnier, F. *Adv. Mater.* **1996**, *8*, 242−245.
(8) Céspedes-Guirao, F. J.; García-Santamaría, S.; Fernández-Lázaro, F.; Sastre-Santos, A.; Bolink, H. J. *J. Phys. D: Appl. Phys.* **2009**, *42*, 105106.
(9) Breeze, A. J.; Salomon, A.; Ginley, D. S.; Gregg, B. A.; Tillmann, H.; Hörhold, H.-H. *Appl. Phys. Lett.* **2002**, *81*, 3085−3087.
(10) (a) Yang, J.; Yoo, H.; Aratani, N.; Osuka, A.; Kim, D. *Angew. Chem., Int. Ed.* **2009**, *48*, 4323−4327. (b) Langhals, H.; Ismael, R. *Eur. J. Org. Chem.* **1998**, 1915−1917. (c) Yoo, H.; Yang, J.; Yousef, A.; Wasielewski, M. R.; Kim, D. *J. Am. Chem. Soc.* **2010**, *132*, 3939−3944.
(11) (a) Han, J. J.; Shaller, A. D.; Wang, W.; Li, A. D. Q. *J. Am. Chem. Soc.* **2008**, *130*, 6974−6982. (b) Fischer, M. K. R.; Kaiser, T. E.; Würthner, F.; Bäuerle, P. *J. Mater. Chem.* **2009**, *19*, 1129−1141. (c) Kim, D.; Osuka, A. *Acc. Chem. Res.* **2004**, *37*, 735−745. (d) García-Parajó, M. F.; Hernando, J.; Mosteiro, G. S.; Hoogenboom, J. P.; van Dijk, E. M. H. P.; van Hulst, N. F. *ChemPhysChem* **2005**, *6*, 819−827. (e) Qian, H.; Negri, F.; Wang, C.; Wang, Z. *J. Am. Chem. Soc.* **2008**, *130*, 17970−17976. (f) Cotlet, M.; Gronheid, R.; Habuchi, S.; Stefan, A.; Barbafina, A.; Müllen, K.; Hofkens, J.; De Schryver, F. C. *J. Am. Chem. Soc.* **2003**, *125*, 13609−13617.
(12) (a) Sildrai, M.; Hadel, L.; Sauers, R. R.; Husain, S.; Krogh-Jespersen, K.; Westbrook, J. D.; Bird, G. R. *J. Phys. Chem.* **1992**, *96*, 7988−7996. (b) Würthner, F. *Chem. Commun.* **2004**, 1564−1579. (c) Ford, W. E.; Kamat, P. V. *J. Phys. Chem.* **1987**, *91*, 6373−6380. (d) Kircher, T.; Löhmannsröben, H.-G. *Phys. Chem. Chem. Phys.* **1999**, *1*, 3987−3992.
(13) (a) Langhals, H.; Jona, W. *Angew. Chem., Int. Ed.* **1998**, *37*, 952−955. (b) Wilson, T. M.; Tauber, M. J.; Wasielewski, M. R. *J. Am. Chem. Soc.* **2009**, *131*, 8952−8957.
(14) (a) Rybtchinski, B.; Sinks, L. E.; Wasielewski, M. R. *J. Phys. Chem. A* **2004**, *108*, 7497−7505. (b) Tauber, M. J.; Kelley, R. F.; Giaimo, J. M.; Rybtchinski, B.; Wasielewski, M. R. *J. Am. Chem. Soc.* **2006**, *128*, 1782−1783.
(15) (a) Davydov, A. S. *Theory of Molecular Exciton*; McGraw-Hill: New York, 1962. (b) Kasha, M.; Rawls, H. R.; El-Bayoumi, M. A. *Pure Appl. Chem.* **1965**, *11*, 371−392.
(16) (a) Bräuchle, C.; Lamb, D. C.; Michaelis, J. *Single Particle Tracking and Single Molecule Energy Transfer*; Wiley-VCH: Weinheim, 2010. (b) Kakitani, T.; Kimura, A. *J. Phys. Chem. A* **2002**, *106*, 2173−2179.
(17) (a) Förster, T. In *Modern Quantum Chemistry*; Sinanoglu, O., Ed.; Academic Press: New York, 1965. (b) Jang, S.; Newton, M. D.; Silbey, R. J. *Phys. Rev. Lett.* **2004**, *92*, 218301.
(18) (a) Ying, L.; Xie, X. S. *J. Phys. Chem. B* **1998**, *102*, 10399−10499. (b) Hernando, J.; van der Schaaf, M.; van Dijk, E. M. H. P.; Sauer, M.; García-Parajó, M. F.; van Hulst, N. F. *J. Phys. Chem. A* **2003**, *107*, 43−52.
(19) Hernando, J.; Hoogenboom, J.; van Dijk, E. M. H. P.; García-Parajó, M. F.; van Hulst, N. F. *J. Lumin.* **2008**, *128*, 1050−1052.
(20) Hernando, J.; Hoogenboom, J. P.; van Dijk, E. M. H. P.; García-López, J. J.; Crego-Calama, M.; Reinhoudt, D. N.; van Hulst, N. F.; García-Parajó, M. F. *Phys. Rev. Lett.* **2004**, *93*, 236404.
(21) Lippitz, M.; Hübner, C. G.; Christ, T.; Eichner, H.; Bordat, P.; Herrmann, A.; Müllen, K.; Basché, T. *Phys. Rev. Lett.* **2004**, *92*, 103001.
(22) Scheblykin, I. G.; Varnavsky, O. P.; Verbouwe, W.; De Backer, S.; Van der Auweraer, M.; Vitukhnovsky, A. G. *Chem. Phys. Lett.* **1998**, *282*, 250−256.
(23) (a) Fornasiero, D.; Kurucsev, T. *J. Chem. Soc., Faraday Trans. 2* **1986**, *82*, 15−19. (b) Spano, F. C. *Acc. Chem. Res.* **2010**, *43*, 429−439. (c) Spano, F. C.; Clark, J.; Silva, C.; Friend, R, H. *J. Chem. Phys.* **2009**, *130*, 074904. (d) Spano, F. C.; Kuklinski, J. R.; Mukamel, S. *Phys. Rev. Lett.* **1990**, *65*, 211−214. (e) Yang, M. *J. Mol. Spectrosc.* **2006**, *239*, 108−114. (f) Ahn, T.-S.; Müller, A. M.; Al-Kaysi, R. O.; Spano, F. C.; Norton, J. E.; Beljonne, D.; Brédas, J.-L.; Bardeen, C. J. *J. Chem. Phys.* **2008**, *128*, 054505.
(24) (a) Ha, J.-H.; Cho, H. S.; Song, J. K.; Kim, D.; Aratani, N.; Osuka, A. *ChemPhysChem* **2004**, *5*, 57−67. (b) Scholes, G. D.; Ghiggino, K. P. *J. Phys. Chem.* **1994**, *98*, 4580−4590.
(25) (a) Yoon, Z. S.; Yoon, M.-C.; Kim, D. *J. Photochem. Photobiol., C: Photochem. Rev.* **2005**, *6*, 249−263. (b) Seibt, J.; Dehm, V.; Würthner, F.; Engel, V. *J. Chem. Phys.* **2007**, *126*, 164308.
(26) (a) Métivier, R.; Nolde, F.; Müllen, K.; Basché, T. *Phys. Rev. Lett.* **2007**, *98*, 047802. (b) Fückel, B.; Köhn, A.; Harding, M. E.; Diezemann, G.; Hinze, G.; Basché, T.; Gauss, J. *J. Chem. Phys.* **2008**, *128*, 074505.
(27) Cho, H. S.; Rhee, H.; Song, J. K.; Min, C.-K.; Takase, M. *J. Am. Chem. Soc.* **2003**, *125*, 5849−5860.
(28) (a) Bartko, A. P.; Dickson, R. M. *J. Phys. Chem. B* **1999**, *103*, 3053. (b) Bartko, A. P.; Dickson, R. M. *J. Phys. Chem. B* **1999**, *103*, 11237. (c) Dickson, R. M.; Norris, D. J.; Moerner, W. E. *Phys. Rev. Lett.* **1998**, *81*, 5322.
(29) (a) Böhmer, M.; Enderlein, J. *J. Opt. Soc. Am. B* **2003**, *20*, 554−559. (b) Dedecker, P.; Muls, B.; Deres, A.; Uji-i, H.; Hotta, J.-i.; Sliwa, M.; Soumillion, J.-P.; Müllen, K.; Enderlein, J.; Hofkens, J. *Adv. Mater.* **2009**, *21*, 1079−1090.
(30) Habuchi, S.; Oba, T.; Vacha, M. *Phys. Chem. Chem. Phys.* **2011**, *13*, 7001−7007.
(31) Vosch, T.; et al. *J. Phys. Chem. C* **2009**, *113*, 11773−11782. (b) Habuchi, S.; Fujita, H.; Michinobu, T.; Vacha, M. *J. Phys. Chem. B* **2011**, *115*, 14404−14415. (c) Schroeyers, W.; et al. *J. Am. Chem. Soc.* **2004**, *126*, 14310−14311.